Structure and dynamics of charged magnetic colloids

2006 J. Phys.: Condens. Matter 18 S2697

(http://iopscience.iop.org/0953-8984/18/38/S12)

INSTITUTE OF PHYSICS PUBLISHING JOURNAL OF PHYSICS: CONDENSED MATTER

J. Phys.: Condens. Matter **18** (2006) S2697–S2711 doi:10.1088/0953-8984/18/38/S12

Structure and dynamics of charged magnetic colloids

J Wagner, B Fischer[1], T Autenrieth[2] and R Hempelmann

Physical Chemistry, Saarland University, D-66123 Saarbrücken, Germany

E-mail: j.wagner@mx.uni-saarland.de

Received 2 May 2006, in final form 17 July 2006
Published 8 September 2006
Online at stacks.iop.org/JPhysCM/18/S2697

Abstract

By coating cobalt ferrite nanoparticles with a silica shell, the polydispersity of the resulting core–shell particles can be reduced. Hereby, opposite to the case for conventional ferrofluids, self-organization to liquid-like and even crystalline structures in aqueous media is enabled. The resulting structures mainly originate from the predominant electrostatic repulsion of colloidal macroions bearing charged groups at the surface of the silica shell. Due to the small magnetic moment of the cobalt ferrite cores, however, these structures can be influenced by external magnetic fields or field gradients. While field gradients act as a magnetic trap for these particles, homogeneous fields induce an aligning of the magnetic momenta. Hereby a decrease of symmetry from spherical to cylindrical symmetry of the structures appearing can be observed. Due to collective phenomena, even interactions significantly smaller than the thermal energy can induce clearly observable structural distortions. Even in the absence of an external field, suspensions of such magnetic particles show an unexpected slow diffusion caused by hydrodynamic interactions.

1. Introduction

Due to the availability of highly defined model systems and their ability of self-organization, colloidal suspensions have attracted substantial interest in science as model systems for condensed matter. Up to now, mainly hard sphere colloids or charged colloidal particles interacting via a screened Coulomb or Yukawa interaction have been investigated [1]. The interaction of both hard sphere and charged particles is purely repulsive and spherically symmetric.

Owing to the spherical symmetry of the monopole potential, the resulting structures also exhibit high symmetry: the liquid-like or glassy structures are spherically symmetric whereas the crystalline bcc and fcc structures exhibit the highest cubic point symmetry $m\bar{3}m$ compatible with translational symmetry.

[1] Present address: Experimental Physics, University Bayreuth, D-95440 Bayreuth, Germany.
[2] Present address: HASYLAB, Deutsches Elektronensynchrotron, D-22603 Hamburg, Germany.

Starting in the 1960s, mesoscopic magnetic particles embedded in a carrier liquid have been stabilizable. These ferrofluids interact via a dipole potential. In contrast to the monopole potential, this pair interaction $V_{ij}^{\mathrm{dip}}(\mathbf{r}_{ij}, \boldsymbol{\mu}_i, \boldsymbol{\mu}_j)$

$$V_{ij}^{\mathrm{dip}}(\mathbf{r}_{ij}, \boldsymbol{\mu}_i, \boldsymbol{\mu}_j) = \frac{\mu_0}{4\pi}\left[\frac{\boldsymbol{\mu}_i.\boldsymbol{\mu}_j}{r_{ij}^3} - 3\frac{(\mathbf{r}_{ij}.\boldsymbol{\mu}_i)(\mathbf{r}_{ij}.\boldsymbol{\mu}_j)}{r_{ij}^5}\right] \tag{1}$$

depends on the relative orientation of the magnetic momenta $\boldsymbol{\mu}_i$, $\boldsymbol{\mu}_j$ and the connecting vector $\mathbf{r}_{ij}$ between two particles and can either be attractive or repulsive. In addition, the orientation of the magnetic moments can be influenced by an external magnetic field. In a sufficiently strong external field $\mathbf{H}$, all momenta arrange parallel to the external field. Under the assumption of equal dipole moments $|\boldsymbol{\mu}_i| = |\boldsymbol{\mu}_j| = \mu$, equation (1) simplifies to

$$V_{ij}^{\mathrm{dip}}(r_{ij}, \theta) = \frac{\mu_0}{4\pi}\frac{\mu^2}{r_{ij}^3}[1 - 3\cos^2\theta] \tag{2}$$

with $\theta = \measuredangle(\mathbf{r}_{ij}, \boldsymbol{\mu}_{i,j}) = \measuredangle(\mathbf{r}_{ij}, \mathbf{H})$ denoting the angle enclosed between the external field and the direction of the connecting vector $\mathbf{r}_{ij}$ as an additional direction dependent parameter. As a consequence, in the field direction, a magnetic attraction, whereas perpendicular to the field direction, a magnetic repulsion, has to be expected. At the magic angle $\theta = \arccos(\sqrt{3}/3)$, the magnetic interaction vanishes at the root of the second Legendre polynomial. Moreover, if the orientation of momenta is random, which can be achieved by magnetic interactions much smaller than the thermal energy $k_{\mathrm{B}}T$ at the next neighbour distance, the overall magnetic interaction vanishes.

Self-organization in colloidal matter can only be observed with sufficiently monodisperse particles. The polydispersity of conventional ferrofluids as colloidal particles with a typical diameter of $\sigma \approx 10$ nm is too high for observing structured suspensions. However, in the region of $\sigma \approx 100$ nm highly defined colloidal particles are known. As a consequence, by the formation of colloidal core–shell particles with an overall diameter of 40 nm $< \sigma <$ 100 nm, the polydispersity can be significantly reduced in order to enable self-organization to liquid-like or even crystalline long range ordered mesostructures.

Through charged groups at the surface of a silica shell, in addition, a screened electrostatic repulsion as the predominant pair interaction is introduced. According to the DLVO theory [2], this Yukawa monopole interaction $V_{ij}^{\mathrm{mono}}(r_{ij})$ is given by

$$V_{ij}^{\mathrm{mono}}(r_{ij}) = \frac{1}{4\pi\varepsilon}\frac{Z_{\mathrm{eff}}^2 e_0^2}{r_{ij}}\exp(-\kappa r_{ij}) \tag{3}$$

with Z_{eff} denoting the number of effective charges and r_{ij} the centre to centre distance of the colloidal macroions. Finally, κ is the inverse Debye screening length depending on the ionic strength in the suspending medium. This quantity consists of an intrinsic part resulting from the counterions of the colloidal macroions and a possible extrinsic part resulting from stray ions in the suspension.

When stray ions are removed by means of a mixed bed ion exchanger, the inverse screening length κ is minimized resulting in a long range electrostatic repulsion. Hence, the mean next neighbour distance is determined by the number density ρ of the colloidal particles and can be approximated as $d_{\max} = \rho^{-1/3}$. Due to the steep decay proportional to r_{ij}^{-3}, for small number densities and large interparticle distances the magnetic interaction becomes small compared to the electrostatic repulsion. Under this condition, the effect of the additional magnetic dipole interaction can be treated within a perturbation formalism of particles interacting via a pure monopole potential.

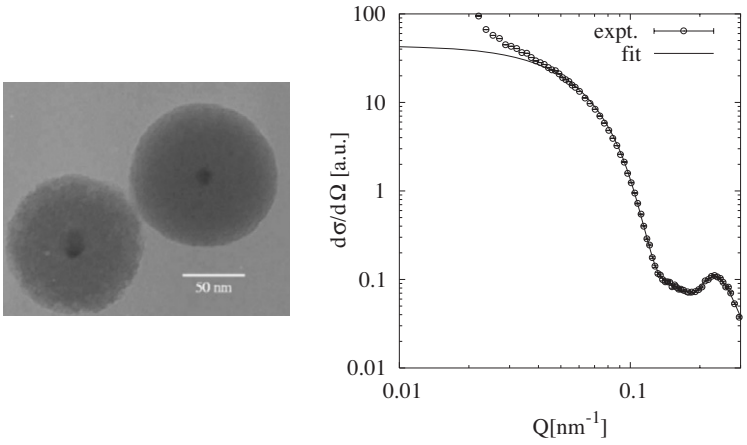

Figure 1. TE micrograph of cobalt ferrite/silica core–shell particles (left-hand side). On the right-hand side, the small angle x-ray scattering of the same particles is displayed. The form factor as obtained from a dilute sample can be described by a polydisperse core–shell model with constant ratio of core to shell diameter. The particles displayed here have a total diameter of $\sigma = 71.3$ nm, a diameter of the magnetic core of $\sigma_c = 14.6$ nm and a polydispersity of $p = 0.131$.

2. Preparation and characterization of cobalt ferrite/silica core–shell particles

Core–shell particles are prepared in a two step procedure. In a first step, the magnetic core is precipitated by addition of a stoichiometric solution of the precursors ferric chloride and cobalt chloride to a solution of potassium hydroxide. The precipitate of the primary particles is washed several times and treated with nitrate. Then, the suspension is flocculated with citric acid and redispersed in water by the addition of tetramethylammonium hydroxide. This dispersion is transferred into ethanol for the subsequent Stoeber process. Hereby, a solution of tetraethoxysilane (TEOS) is dropped under stirring for several hours into the suspension of the core particles. The polycondensation of TEOS around the magnetic cores in the presence of catalytic amounts of aqueous NH_3 is indicated by the increasing turbidity of the suspension. The thickness of the shell can be tuned by the amount of TEOS used in this reaction. Finally, the resulting suspension is cleaned by dialysis against distilled water for one week in order to remove stray ions.

While the thickness of the shell can be tuned in order to obtain particles with an overall diameter of 40 nm $< \sigma <$ 100 nm, the maximum size of the magnetic core is limited to $\sigma_c \approx 15$ nm. For larger magnetic particles, the dipolar attraction becomes significantly larger than the thermal energy. Probably existing larger particles, however, cannot be redispersed after the first precipitation.

The resulting particles consist of a single $CoFe_2O_4$ core embedded in a silica shell. This topology can easily be seen employing TEM (figure 1, lhs). The core–shell structure also becomes evident from small angle x-ray scattering experiments [3]. In contrast to the direct imaging TEM probing only a few particles, in scattering experiments the statistical average of a macroscopic ensemble is determined. The particles used here have an overall diameter of $\sigma = 71.3$ nm, a core diameter $\sigma_c = 14.6$ nm and polydispersity defined by

$$p = \sqrt{\frac{\langle \sigma^2 \rangle - \langle \sigma \rangle^2}{\langle \sigma \rangle^2}} \tag{4}$$

of $p = 0.131$. This is considerably lower than for standard ferrofluids with $p \gtrsim 0.30$.

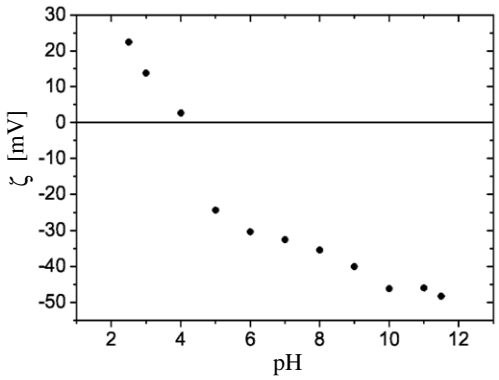

Figure 2. ζ potential of cobalt ferrite/silica core–shell particles depending on the pH. The point of zero charge at pH = 4.5 indicates the presence of weakly acidic groups at the silica surface.

The existence of negative charges at the surface of the silica shell is evident from the ζ potential. The isoelectric point at pH $=$ 4.5 (figure 2) indicates that the charge results from weakly acidic groups, whose dissociation strongly depends on the local pH and therefore on the number density of the particles. In the presence of a mixed bed ion exchanger, the counterions of the colloidal particles are protons. Hence, the increased number of particles influences the structure of the counterion cloud surrounding the colloidal macroions. Hereby, also the dissociation of the weakly acidic ≡Si–OH surface groups is changed. Nevertheless, in neutral pH a potential of $\zeta = -35$ mV is typical for these particles [4].

The presence of a magnetic moment in these particles can easily be seen by eye from the interaction of colloidal crystals with a magnetic field gradient. Such a gradient $\nabla\mathbf{H}$ present at a singularity like the edge of a permanent magnet causes a force $\mathbf{F} \propto \mu\nabla\mathbf{H}$ on the core–shell particles bearing a magnetic moment μ. Hereby, the particles are attracted towards increasing field gradient, i.e. towards the edge of a permanent magnet acting as a magnetic trap. As a consequence, the number density of colloidal particles increases near the edge of a magnet pole. If the colloidal particles are arranged in a lattice whose lattice constants are comparable to the wavelength of visible light, this mesostructure induces Laue scattering of visible light. Hereby, crystals select, under a given angle of observation, wavelengths fulfilling Bragg's law. With the human eye as an energy dispersive detector, coloured Bragg spots can be observed. With increasing number density, the lattice constant decreases. Hence, colloidal crystals with large particle densities fulfil the Bragg condition at the same angle of observation for shorter wavelengths than isomorphous structures with lower density. Hence a colour shift of the Laue spots from red to blue in the vicinity of the magnetic singularity indicates a magnetophoresis towards increasing field gradient (figure 3).

The magnetic behaviour of the core–shell particles also becomes evident from the magnetization of the suspensions. By analysis of the field dependent magnetization, i.e. magnetogranulometry, the size distribution of the magnetic cores can be obtained. Hereby the interaction of the colloidal particles with an external, homogeneous magnetic field is investigated. Since in our systems, the magnetic cores are well separated by the charged silica shell, the magnetic interparticle interaction can in dilute samples be neglected to a very good approximation. Hence, for every class of sizes, a Langevin behaviour has to be expected. Assuming a spherical shape of the cores and a Schulz–Flory size distribution of the cobalt ferrite cores, their median size and polydispersity can be determined as described in

Figure 3. Magnetophoresis of cobalt ferrite/silica core–shell particles in the presence of a field gradient originating from the permanent magnet at the right-hand side. In the vicinity of the maximum field gradient, the lattice constant of the colloidal crystals decreases. As consequence, a shift of the backscattered light from red to blue colour can be observed. The dark spheres are ion exchanger resin.

(This figure is in colour only in the electronic version)

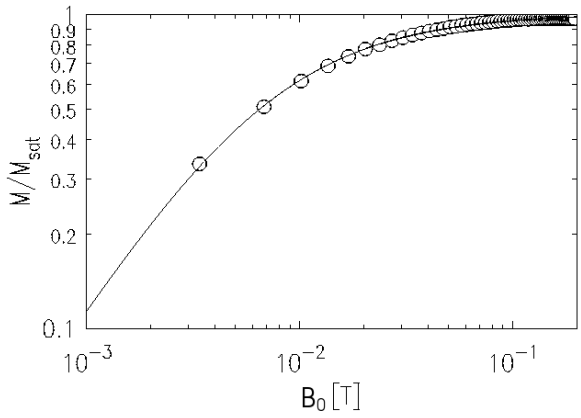

Figure 4. Relative magnetization for a suspension of cobalt ferrite/silica core–shell particles. The magnetic diameter of the core has $\langle\sigma_{c,mag}\rangle = 14.3$ nm in surprising coincidence with the topological diameter of $\langle\sigma_c\rangle = 14.6$ nm determined from SAXS. The absolute saturation magnetization is due to the small magnetic volume fraction occupied by the cobalt ferrite cores, typically as low as $M_S = 100$ A m^{-1}.

detail in [5]. In contrast to the case for conventional ferrofluids with ubiquitous clusters, the experimental magnetization data for silica coated particles can very well be described by this formalism. However, due to the extremely small magnetic volume fraction of the cobalt ferrite cores in the range of $\phi_{mag} \approx 10^{-4}$, the saturation magnetization for typical suspensions is as low as $M_S = 100$ A m^{-1}.

The best parameters for the particle size distribution are in surprising coincidence with the topological ones obtained from SAXS experiments. From the least squares fit displayed in figure 4, the optimum parameters $\langle\sigma_{c,mag}\rangle = 14.3$ nm with a polydispersity of $p = 0.28$ are obtained, which is still small compared to those for conventional ferrofluids.

Particles of hard magnetic cobalt ferrite in this regime of size exhibit a permanent magnetic moment even in the absence of an external field due to the strong spin–lattice coupling indicated

by a high magnetic anisotropy energy. As consequence, the core particles used for this system perform a Brownian relaxation process in an alternating magnetic field [6, 7].

3. Field induced anisotropy of liquid-like ordered suspensions

Due to the small ratio of core size to core separation, the magnetic interaction is significantly smaller than the thermal energy. As a consequence, in the absence of an external field, a random orientation of the magnetic momenta can be expected. Under this condition, the average magnetic interaction vanishes: the structure of a liquid-like ordered suspension of core–shell particles shows spherical symmetry. The resulting structure factors can be described assuming a pure electrostatic monopole potential within the rescaled mean spherical approximation [8, 9]. In figure 5 the structure factors of two liquid-like ordered suspensions at different number densities are displayed. The two samples consist of the same particles with an overall diameter of $\sigma = 41.3$ nm. By reducing the thickness of the silica shell, the magnetic interaction is enhanced, the topological polydispersity, however, is increased. The lines represent least squares fits employing RMSA assuming a Yukawa interaction for monodisperse particles. In the presence of a mixed bed ion exchanger in sealed quartz capillaries quantitatively removing stray ions, only the presence of protons, the counterions of the colloidal macroions, is assumed for the calculation of the Debye screening length. In the more concentrated sample, at a number density of $\rho = 2.10 \times 10^{20}$ m^{-3} the next neighbour distance is $d = 3.6\sigma$, whereas in the dilute suspension at a number density of $\rho = 9.84 \times 10^{19}$ m^{-3} this distance rises to $d = 4.3\sigma$. Although the two samples consist of identical particles and are identically prepared, the numbers of effective charges are significantly different. While in the dilute case the best parameter for the number of effective charges is $Z_{\mathrm{eff}} = 51$, this quantity increases for the concentrated sample by a factor 3/2 to $Z_{\mathrm{eff}} = 77$. This effect demonstrates the dependence of the dissociation of weakly acidic functional groups on the local structure of the cloud of counterions around the central macroion, which is highly influenced by their number density.

Nevertheless, this experiment demonstrates the ability of the weakly charged silica shell to keep the particles distant by mutual repulsion. Hereby, the mean interparticle distance is solely determined by the number density of colloidal particles.

In the presence of an external field, however, due to the orientation of the magnetic momenta parallel to the external field, a small magnetic attraction in field direction and a small magnetic repulsion perpendicular to the field direction should disturb the spherical symmetry of the sample. As a consequence a lower symmetry according to the cylinder symmetry of the dipole–dipole potential is observed. Hereby, with the magnetic field perpendicular to the incident beam, i.e. in the plane of the scattering vector $\mathbf{Q}$, an anisotropic section is observed (figure 6, middle). When the external field is applied parallel to the incident beam, i.e. perpendicular to the plane of the scattering vector $\mathbf{Q}$, however, a radially symmetric section is observed (figure 6, rhs).

In order to maximize the dipole–dipole interaction in the suspension, for these experiments particles with a comparatively thin silica shell with an overall diameter of $\sigma = 41.3$ nm were used. For spherical particles, the scattered intensity can be factorized according to

$$I(\mathbf{Q}) \propto S(\mathbf{Q})P(Q), \tag{5}$$

whereby the form factor $P(Q)$ accounts for intraparticle correlations and the structure factor $S(Q)$ describes the interparticle correlations, i.e. the mesoscale structure of the colloidal liquid. Whereas the former quantity $P(Q)$ describing the single particle scattering is, due to the spherical topology of the core–shell particles, radially symmetric, the latter quantity $S(\mathbf{Q})$ can

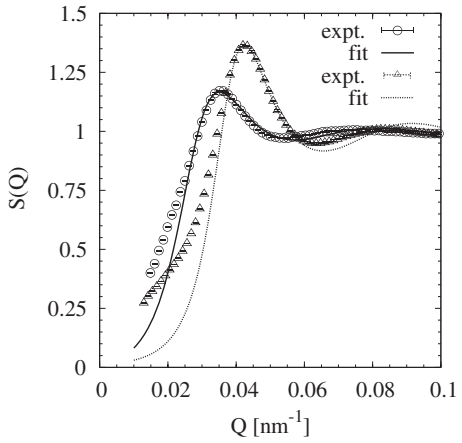

Figure 5. Structure factors of liquid-like ordered suspensions of cobalt ferrite/silica core–shell particles with an overall diameter of $\sigma = 41.3$ nm in the absence of an external magnetic field. Due to the small magnetic interaction $V_{ij}^{\mathrm{mag}} \ll k_{\mathrm{B}}T$ isotropic structures are observed. The structure factors can be described by the rescaled mean spherical approximation (RMSA). The open circles result from a suspension with $\rho = 9.84 \times 10^{19}$ m^{-3}, the triangles from a suspension with $\rho = 2.10 \times 10^{20}$ m^{-3}.

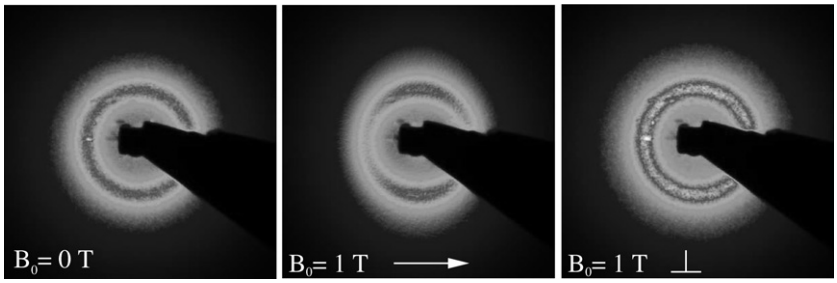

Figure 6. Small angle x-ray scattering patterns resulting from liquid-like ordered suspensions of cobalt ferrite/silica core–shell particles. At the left-hand side, without an external field a spherically symmetric pattern is visible. In the middle and on the right-hand side, two sections of a cylindrical symmetric scattering pattern are displayed. With a magnetic field perpendicular to the incident beam (i.e. the horizontal direction in the plane of detection), an anisotropic pattern appears (middle), whereas with a field parallel to the incident beam (i.e. perpendicular to the plane of detection), a radially symmetric section can be observed (rhs).

due to dipole interactions become angle dependent. For a sufficiently dilute and electrostatically screened suspension with the structure of an ideal gas, the structure factor is by definition $S(Q) \equiv 1$. Hence, the division of the scattering resulting from a concentrated suspension by that of a dilute suspension is the structure factor of the concentrated suspension times the ratio of concentrations.

The angle dependent analysis of the structure factor $S(Q)$ in sectors centred (i) parallel, (ii) perpendicular and (iii) at the magic angle $\theta = \arccos(\sqrt{3}/3)$ to the field is displayed in figure 7. Whereas in the absence of an external field, all data coincide within the experimental accuracy, with a field perpendicular to the incident beam, a significant dependence on $\theta = \measuredangle(\mathbf{Q}, \mathbf{H})$ is observed. Hereby, the amplitude of $S(\mathbf{Q})$ increases perpendicular to the external field and decreases parallel to the external field. In the magic sector, at vanishing dipolar pair interaction,

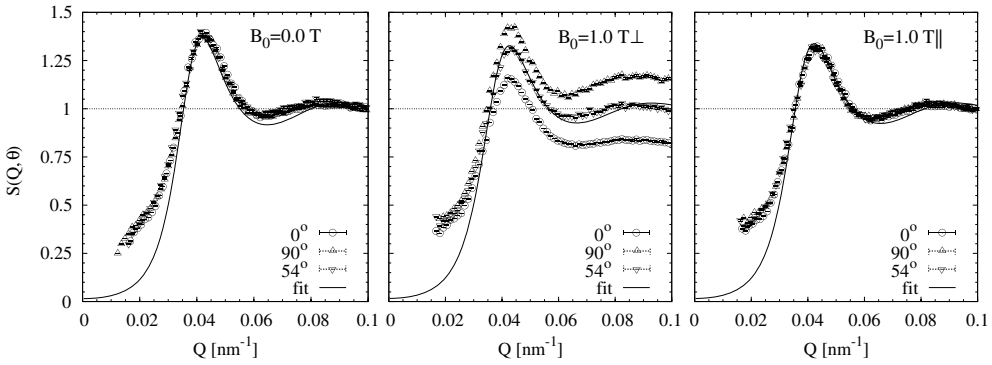

Figure 7. Angle dependent structure factor $S(Q,\theta)$. The symbols represent averages of sectors centred at (i) $\theta = 0$, (ii) $\theta = \pi/2$ and (iii) $\theta = \arccos(\sqrt{3}/3)$ that cover an angular interval of $\pm 10°$. In the absence of an external field, all sectors coincide within the experimental accuracy (left). The same can be observed if a field is applied parallel to the incident beam (right). However, in the presence of a field perpendicular to the incident beam (middle), significant differences are observed. While the sector centred at the magic angle is not affected, the experimental $S(Q,\theta = \pi/2)$ (perpendicular to the field) increases and $S(Q,\theta = 0)$ (parallel to the field) decreases. The position of the maximum remains unchanged with respect to the modulus of the scattering vector $|\mathbf{Q}|$.

the amplitude of $S(\mathbf{Q})$ is not affected by the external field. Hence, even in the presence of an external field perpendicular to the direction of the incident beam, the structure factor in this sector can be described using the RMSA assuming a monopole Yukawa potential. The position of the maximum in $S(\mathbf{Q})$ indicating the next neighbour distance remains unchanged with respect to θ. This indicates that the mean particle interdistances do not change, whereas the degree of order becomes a function of θ.

Since the monopole interaction is much larger than the dipole interaction, a perturbation approach can be used to describe the anisotropic structure factors in the presence of an external field. Since the formation of liquid-like structures is a many particle problem, in addition to the pair potential, interactions mediated by other particles have to be taken into account. Theories describing the structure of liquids as a response to a given interaction potential are based on the Ornstein–Zernike (OZ) equation that can for spherically symmetric problems be written as

$$h(r) = c(r) + \rho \int c(|\mathbf{r} - \mathbf{r}'|)h(r')\,\mathrm{d}^3r'. \tag{6}$$

The OZ equation connects the total correlation function $h(r) = g^{(2)}(r) - 1$ to the direct correlation function $c(r)$, whereby many particle interactions are described by the convolution integral in equation (6). This equation implies, due to recursion, an infinite power series in terms of the number density ρ for the total correlation function $h(r)$. In order to get a closed set of equations, the diagrammatic cluster expansion is truncated for small clusters. By this approximation a closure relation is obtained that connects the pair potential to the direct correlation function. Within the mean spherical approximation (MSA) [10],

$$c(r) = -\beta V_{ij}(r_{ij}) \qquad r > \sigma \tag{7}$$

for non-overlap distances $r_{ij} > \sigma$, the direct correlation function is just proportional to the pair potential $V_{ij}(r_{ij})$ with $\beta = 1/(k_\mathrm{B}T)$ denoting the inverse thermal energy. This leads in combination with the OZ equation to a linear integral equation, for that semianalytical solutions exist for the Yukawa potential [8] and for the hard sphere dipolar potential [11].

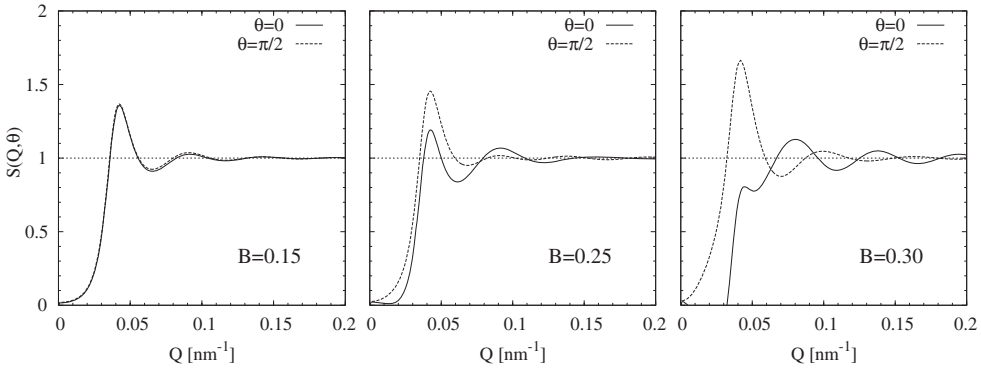

Figure 8. Structure factors for a dipolar Yukawa system calculated within the rescaled mean spherical approximation (RMSA). Compared to a Yukawa system, the additional parameter $B = \mu_0\mu^2/(4\pi k_B T\sigma^3)$ as the reduced magnetic interaction is required. In agreement with the experiment, the maximum in $S(Q, \theta)$ remains unchanged with respect to the modulus of the scattering vector Q for small magnetic interactions. For the largest interaction with $B = 0.30$, only a small shoulder remains in the direction of the external field, whereas the former second harmonic is now the global maximum indicating a reduced mean interparticle distance. $\theta = 0$ hereby denotes the direction parallel and $\theta = \pi/2$ the direction perpendicular to the external field.

In order to calculate the angle dependent structure factor for a sum of a Yukawa potential and a dipole–dipole potential, the potential, the closure relation and the OZ equation have to be expanded into rotational invariants. Due to symmetry properties of the coupling coefficients involved, it can be shown that the spherically symmetric monopole contribution decouples from the cylindrical symmetric dipole–dipole contribution [12]. As a consequence the structure factor for a system of charged magnetic particles is just the sum of the MSA structure factor of a Yukawa liquid and the anisotropic part of the hard sphere dipolar liquid.

It is well known that within the MSA the hard sphere exclusion is underestimated. As a consequence, for dilute, strongly repelling systems, the pair correlation function $g^{(2)}(r)$ becomes negative at the limit $r \to \sigma^+$. Hansen proposed a rescaling procedure to circumvent this unphysical result: here, the real system is replaced by a virtual system with the same number density and particles increased by a factor $\xi > 1$. This leads to a drastic increase of the apparent volume fraction to $\phi' = \phi\xi^3$ enhancing the effective hard sphere exclusion. In order to keep the interaction in the rescaled system constant, the potential parameters are rescaled according to ξ [9]. The rescaling parameter ξ is determined by transformation of the structure factor to $g^{(2)}(r)$ preserving the positive definiteness through the condition $g^{(2)}(r \to \sigma^+) = 0$.

To include dipole–dipole interactions, in addition to the number of charges and the inverse Debye screening length for the Yukawa part, a magnetic interaction parameter is required, that can be defined by the reduced quantity

$$B = \frac{\mu_0}{4\pi}\frac{\mu^2}{\sigma^3 k_B T}. \tag{8}$$

This quantity equals the magnetic repulsion for particles at contact distance with the connecting vector perpendicular to the field direction in units of the thermal energy. Due to the soft concurrent Yukawa potential, whose curvature is extremely low near the equilibrium position, even very small dipolar perturbations can significantly influence the structure factor (figure 8). In accordance with the experimental result, this theoretical approach predicts an unshifted position of the maximum in $S(Q, \theta)$ with respect to the modulus of the scattering vector Q.

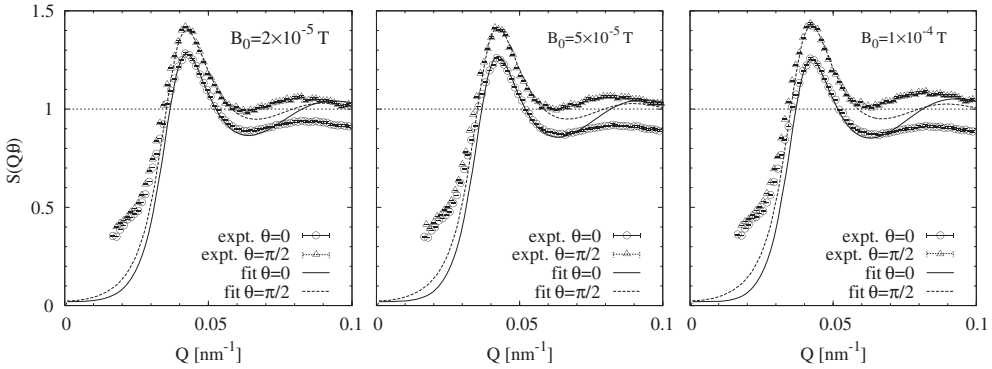

Figure 9. Experimental structure factors $S(Q, \theta)$ from sectors parallel ($\theta = 0$) and perpendicular to the external field ($\theta = \pi/2$). With increasing strength of the external field, the gap between these sectors increases. While the region of the coordination peak is well described using the RMSA assuming a dipolar Yukawa interaction, at large Q, discrepancies between experiment and theory are observed. In this region of scattering vectors, distances closer than the next neighbour distance in real space are probed. A possible reason for this discrepancy between theory and experiment is the non-negligible polydispersity of the magnetic cores that is not included in this theoretical approach.

When the magnetic interaction is further increased, the former maximum decreases to a small shoulder in the direction parallel to the field. The former second harmonic is in this case the new global maximum. Since this global maximum appears at a larger scattering vector Q, in real space, the mean interparticle distance is reduced in the direction parallel to the external field.

A quantitative comparison of theory and experiment is displayed in figure 9 for different strengths of the magnetic field. The projection of the magnetic moments in the direction of the external field increases according to the magnetization curve. As a consequence, the effective magnetic interaction parameter increases until the saturation plateau is reached: the anisotropy, as is visible in the gap between $S(Q, \theta = 0)$ and $S(Q, \theta = \pi/2)$, increases with the external field and reaches a limit in the saturation regime.

While the experimental data are well described in the region of the maximum of $S(Q)$, i.e. in real space at the distance from a central particle to its coordination shell, deviations at small and high Q are observed. It is well known that topological polydispersity increases the compressibility of the suspension, which is proportional to the limit $S(Q \to 0)$ [13, 14]. In the present systems, in addition a non-negligible polydispersity in terms of the core dipole moments is obvious. Due to the steep r_{ij}^{-3} dependence of the dipole–dipole potential, effects of the magnetic polydispersity are important at small interparticle distances, i.e. in Fourier space at large Q. Hence, the magnetic polydispersity not included in the theoretical approach used here is a possible reason for the discrepancies between theory and experiment at large Q.

In figure 10, the difference between the amplitudes of the structure factors perpendicular and parallel to the external field $S(Q_{\max}, \theta = \pi/2) - S(Q_{\max}, \theta = 0)$ at the peak position $Q_{\max} = 4.2 \times 10^{-2}$ nm^{-1} is displayed. At $H = 10^{-2}$ T, a plateau of saturation is reached. This limit excludes field inhomogeneities as a possible reason for the observed anisotropy: inhomogeneities increase with the strength of the applied field. Hence, effects related to inhomogeneities would continuously increase with the field. In contrast, the limit here is reached in the regime of the saturation magnetization. Even very small fields can, due to collective phenomena, induce a significant anisotropy.

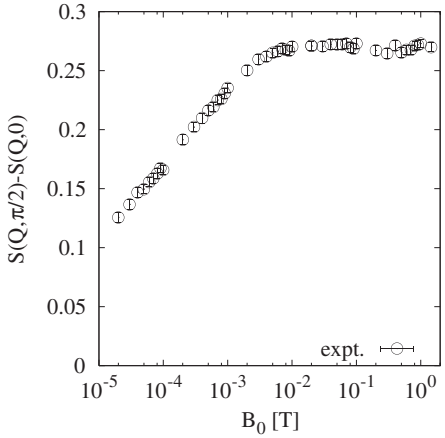

Figure 10. Difference of the structure factors $S(Q_{\max}, \theta = \pi/2) - S(Q_{\max}, \theta = 0)$ in the sectors perpendicular and parallel to the external field at the coordination maximum at $Q_{\max} = 4.2 \times 10^{-2}$ nm^{-1}. Due to collective phenomena even tiny magnetic fields can induce anisotropic structures. In the region of the saturation magnetization, at several milliteslas a limit is reached.

4. Collective diffusion

The structural relaxation time can be estimated as the time needed by a particle to move by a diffusive motion one particle diameter away from its origin $\tau = \langle\sigma^2\rangle/(6D)$. For a colloidal particle with a diameter of $\sigma = 100$ nm in water at room temperature, this time is $\tau = 0.4$ ms. Hence, this process is too slow for neutron spin echo spectroscopy and can only be observed by means of correlation spectroscopy. Concentrated, interacting suspensions of magnetic core–shell particles, however, are black and thus opaque for optical wavelengths. Hence, scattering experiments employing visible light as a probe are not possible in concentrated systems. A method for circumventing this limitation is the use of coherent x-rays accessible at third generation synchrotron sources [15].

Since the smallest distance that can be probed by a scattering experiment is half of the wavelength used, with x-rays there is practically no limitation in the accessible Q range for colloidal samples. Using visible light, interdistances of interest can often not be accessed due to this limitation.

Using x-ray correlation spectroscopy (XPCS), the collective diffusion of opaque colloids can be probed at mesoscopic scales of space and time. With this technique, in a homodyne experiment, the intensity autocorrelation function $g_2(Q, t)$ is determined; this is defined as

$$g_2(Q,t) = \frac{\langle I(Q,t+\tau)I(Q,\tau)\rangle_\tau}{\langle I(Q,\tau)\rangle_\tau^2} = 1 + A(Q)|g_1(Q,t)|^2. \tag{9}$$

Hereby, the contrast $A(Q)$ depends on the coherence properties of the source and the solid angle covered by the active detector size. Whereas in a photon correlation experiment with coherent laser radiation and sufficiently small detector size the contrast is $A(Q) \approx 1$, this quantity is in a XPCS experiment, due to the small coherence length of x-rays, typically much smaller ($A(Q) \approx 0.05{-}0.1$).

The quantity $g_1(Q, t)$ in equation (9) is the field autocorrelation function that can for a Gaussian diffusion process of non-interacting, equally sized spheres be expressed as a single exponential decay

$$g_1(Q,t) = \exp[-\Gamma(Q)t] = \exp[-Q^2 D(Q)t] \tag{10}$$

with the relaxation constant $\Gamma(Q) = Q^2 D$. For a system of non-interacting spherical particles with a hydrodynamic diameter σ_H suspended in a medium with the viscosity η, the collective diffusion coefficient $D(Q)$ equals the single particle Stokes–Einstein self-diffusion coefficient

$$D(Q) \equiv D_0 = \frac{k_B T}{3\pi \eta \sigma_H}. \tag{11}$$

In an interacting system, however, non-Gaussian diffusion processes take place. Such non-Gaussian diffusion processes can formally be described by a time dependent diffusion coefficient $D(Q, t)$. In the limit of short times, however, a time independent collective diffusion process is observed with the effective diffusion coefficient

$$D_{\text{eff}}(Q) = \lim_{t \to' 0'} D(Q, t), \tag{12}$$

where the notation $t \to' 0'$ indicates the coarse grain limit for a timescale larger than the momentum relaxation time τ_B. As a consequence, according to equation (10) the effective diffusion coefficient can be obtained from the first cumulant of the field autocorrelation function [16].

The effective diffusion coefficient in an interacting system is influenced by direct interactions and indirect, hydrodynamic interactions (HI). Whereas the former ones are caused by the instantaneous pair interactions, the latter ones are mediated by flow patterns in the suspending medium. The effective diffusion coefficient can be written as an extension of the de Gennes narrowing [17] as

$$D_{\text{eff}}(Q) = \frac{D_0}{S(Q)} H(Q), \tag{13}$$

where the additional factor, the hydrodynamic function $H(Q)$ [18], is connected to the diffusion tensors $\mathbf{D}_{ij}(\mathbf{r}^N)$ by

$$H(Q) = \frac{1}{Q^2 D_0} \left\langle \sum_{i=1}^{N} \sum_{j=1}^{N} \mathbf{Q} \cdot \mathbf{D}_{ij}(\mathbf{r}^N) \cdot \mathbf{Q} \exp[\mathrm{i}\mathbf{Q} \cdot (\mathbf{r}_i - \mathbf{r}_j)] \right\rangle. \tag{14}$$

While in hard sphere systems, HI in general lead to a slowing down of diffusion ($H(Q) < 1$) [19], in highly ordered, dilute systems an enhancement ($H(Q) > 1$) of collective diffusion near the correlation maximum is also observed [20].

In figure 11, the relaxation rates for non-interacting core–shell particles in a highly dilute ($\phi = 10^{-4}$) suspension (open circles) determined by PCS and the relaxation rates for an opaque, moderately concentrated suspension ($\phi = 0.027$) determined by means of XPCS are displayed. For these experiments, particles with an overall diameter of $\sigma = 71.3$ nm and a core diameter of $\sigma_c = 14.6$ nm with a topological polydispersity of $p = 0.131$ are used. While for the highly dilute suspension a simple proportionality to Q^2 is visible, for the more concentrated one significant deviations from this simple behaviour that indicate a Gaussian diffusion process can be observed [5]. From the slope of the relaxation rates of the non-interacting, highly dilute sample, D_0 can be experimentally obtained.

In figure 12 the structure factor of this spherically symmetric, liquid-like ordered suspension, together with the inverse effective diffusion coefficient $D_0/D_{\text{eff}}(Q)$, is displayed. The two quantities show characteristic peaks with coinciding maximum. According to equation (13), the two curves should superimpose in the absence of HI, i.e. $H(Q) \equiv 1$. The deviations, however, indicate a tremendous slowing down of the collective diffusion caused by hydrodynamic interactions.

The hydrodynamic function $H(Q)$ (figure 13) is for this system much lower than theoretically expected for a system in this range of concentration. HI are highly affected by

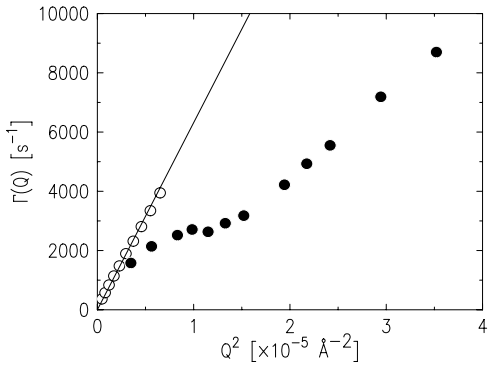

Figure 11. Relaxation rates for a highly dilute ($\phi = 10^{-4}$) suspension obtained by means of dynamic light scattering (open circles) and the ones for a suspension of moderate concentration ($\phi = 0.027$) determined using XPCS (filled circles). The solid line is a fit of the relaxation rates with zero intercept, whose slope represents the free diffusion coefficient D_0.

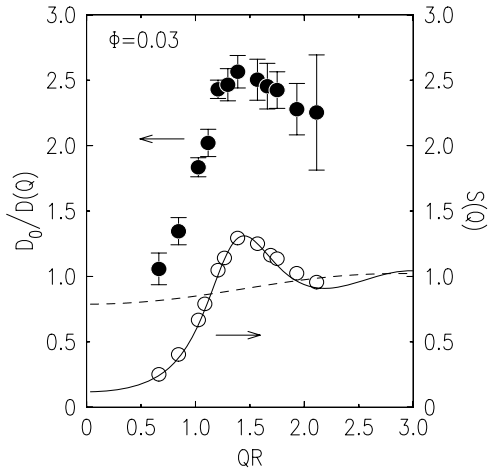

Figure 12. Structure factor $S(Q)$ (open circles) and inverse effective diffusion coefficient $D_0/D_{\text{eff}}(Q)$ (filled circles) of a liquid-like ordered suspension of core–shell particles in the absence of an external field. The solid line is a RMSA fit. For comparison a calculated structure factor for a hard sphere system with the same volume fraction is represented as a dashed line. Without HI, the curves would superimpose.

multiparticle contributions. For a calculation of this quantity, in general the total configuration of the system must be known. For highly dilute systems, however, the diffusion tensors in equation (14) can be approximated by Rotne–Prager tensors, which depend only on the pair correlations. This pairwise additive approach [18] describes HI in dilute, charged systems with surprising accuracy [20].

In concentrated hard sphere systems, however, HI lead even in the correlation maximum to a slowing down of collective diffusion. This is predicted by the multiparticle $\delta\gamma$ approach of Beenakker and Mazur [21]. This theory was originally developed for hard spheres. As input for this theory, however, only the volume fraction and the structure factor are required. Using the experimental structure factor as an input, the $\delta\gamma$ expansion can be adapted to the present charge stabilized system.

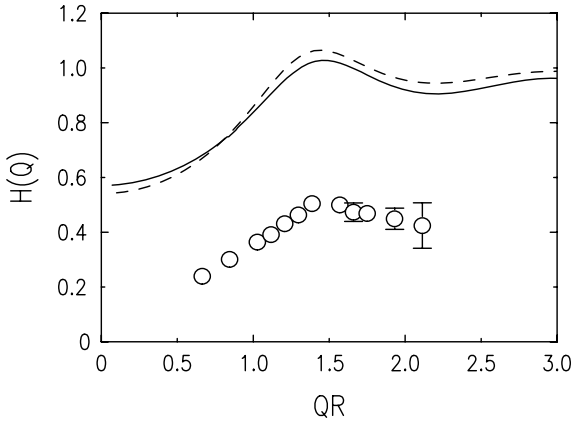

Figure 13. Hydrodynamic function $H(Q)$ for a liquid-like ordered system of magnetic core–shell particles. The experimental data (open circles) are significantly overestimated by the existing theoretical approaches: the $\delta\gamma$ expansion using the experimental $S(Q)$ as input is represented as a solid line, whereas the pairwise additive approximation is represented by the dashed line.

Both existing theories overestimate the experimental data by a factor of at least two. The $\delta\gamma$ expansion mimics well the Q dependence of $H(Q)$ that depends on the collective term of the hydrodynamic function. It fails, however, to predict the self-part, i.e. the limit $H(Q \to \infty)$. As a consequence, the reason for this unexpected slowing down of diffusion is a phenomenon independent on the scattering vector Q.

5. Conclusion

With the cobalt ferrite/silica core–shell particles, a colloidal magnetic Yukawa system is available that self-organizes to three dimensional, mesoscale structures. This system enables the investigation of a small dipolar perturbation of a soft, repelling monopole potential. Even magnetic interactions much less than the thermal energy can induce a clearly detectable structural anisotropy in the presence of an external field. Neglecting the magnetic polydispersity of the particles, these effects can be described with RMSA employing a magnetic Yukawa potential. Hereby, the experimental result of unchanged equilibrium interdistances for small magnetic interactions is theoretically confirmed.

By means of XPCS the collective diffusion coefficient of these opaque suspensions is accessible. Experiments using such systems, even in the absence of an external field, show an unexpected slow diffusion. This effect is induced by hydrodynamic interactions. Available theories overestimate the self-part of the hydrodynamic function $H(Q)$ at least by a factor of 2.

The experimental access to a model system with stronger magnetic interactions should enable the study of structures with increased anisotropy in the regime of changing equilibrium interdistances. In this regime, experimental access to differences in the diffusion parallel and perpendicular to an external field is possible within the currently available time resolution of coherent x-ray scattering.

Acknowledgments

The authors thank colleagues from the ESRF, Grenoble (France), especially A Robert and T Narayanan, for support during many experiments at the beamlines ID10A and ID02.

Financial support by the Deutsche Forschungsgemeinschaft within the priority programme SPP 1104 is gratefully acknowledged.

References

[1] Pusey P N 1991 *Colloidal Suspensions in Liquids, Freezing and Glass Transition* (Amsterdam: Elsevier)
[2] Verwey E J W and Overbeek J T G 1948 *Theory of the Stability of Lyophobic Colloids* (Amsterdam: Elsevier)
[3] Wagner J 2004 Small angle scattering from spherical core–shell particles: an analytical scattering function for particles with Schulz–Flory size distribution *J. Appl. Crystallogr.* **37** 750–6
[4] Autenrieth T, Wagner J, Hempelmann R, Härtl W, Robert A and Grübel G 2004 Cobalt ferrite silica core/shell particles: a magnetic Yukawa system *Appl. Organomet. Chem.* **18** 520–2
[5] Robert A, Wagner J, Autenrieth T, Härtl W and Grübel G 2005 Structure and dynamics of electrostatically interacting magnetic nanoparticles in suspension *J. Chem. Phys.* **122** 084701
[6] Fischer B, Wagner J, Schmitt M and Hempelmann R 2005 Tuning the relaxation behaviour by changing the content of cobalt in $Co_xFe_{3-x}O_4$ ferrofluids *J. Phys.: Condens. Matter* **17** 7875–83
[7] Fischer B, Wagner J, Schmitt M, Trieu V and Hempelmann R 2006 Dependence of Brownian relaxation on the volume fraction and an external field *Z. Phys. Chem.* **220** 69–77
[8] Hayter J B and Penfold J 1981 *Mol. Phys.* **42** 108
[9] Hansen J P and Hayter J B 1982 *Mol. Phys.* **46** 651
[10] Waismann E and Lebowitz J L 1972 Mean spherical model integral equation for charged hard spheres *J. Chem. Phys.* **56** 3086–99
[11] Wertheim M S 1971 Exact solution of the mean spherical model for fluids of hard spheres with permanent electric dipole moments *J. Chem. Phys.* **55** 4291–8
[12] Wagner J, Fischer B and Autenrieth T 2006 Field induced anisotropy of charged magnetic colloids: a rescaled mean spherical approximation study *J. Chem. Phys.* **124** 114901
[13] Klein R and D'Aguanno B 1996 *Light Scattering, Principles and Development* (Oxford: Oxford) Chapter (Static Scattering Properties of Colloidal Suspensions) pp 30–102
[14] Härtl W and Versmold H 1984 *J. Chem. Phys.* **80** 1387
[15] Robert A, Wagner J, Autenrieth T, Härtl W and Grübel G 2005 Coherent x-rays as a new probe for the investigations of the dynamics of opaque colloidal suspensions *J. Magn. Magn. Mater.* **289** 47–9
[16] Berne B J and Pecora R 2000 *Dynamic Light Scattering* (New York: Dover)
[17] De Gennes P G 1959 Liquid dynamics and inelastic scattering of neutrons *Physica* **25** 825–39
[18] Nägele G and Baur P 1997 Long-time dynamics of charged colloidal suspensions: hydrodynamic interaction effects *Physica* A **245** 297
[19] van Megen W, Ottewill R H, Owens S M and Pusey P N 1985 Measurement of the wave-vector dependent diffusion coefficient in concentrated particle dispersions *J. Chem. Phys.* **82** 508–15
[20] Härtl W, Beck C and Hempelmann R 1999 Determination of hydrodynamic properties in highly charged colloidal systems using static and dynamic light scattering *J. Chem. Phys.* **110** 7070–72
[21] Beenakker C W J and Mazur P 1984 Diffusion of spheres in a concentrated suspension ii *Physica* A **126** 349–70